A new insight into microseepage model using detailed spectroscopy: a case study from Qom area, Iran

Saeid Asadzadeh [1]
Carlos Roberto de Souza Filho [1]

[1] Universidade Estadual de Campinas - UNICAMP
Caixa Postal - 13083-970 - Campinas - SP, Brazil
saeid@ige.unicamp.br
beto@ige.unicamp.br

Abstract. The near-vertical leakage of light gaseous hydrocarbons (HC) to the surface triggers an array of diagenetic physio-chemical and mineralogical changes in the soils and sediments overlying a HC accumulation. Over years, multi-, and hyperspectral remote sensing has been used to detect the mineralogic footprints of microseepage systems using their diagnostic spectral features in the visible-near infrared (VNIR) and shortwave infrared (SWIR) wavelengths. In practice, however, there has been ambiguities in result interpretation because the diversity and quantity of the target minerals was not well delineated by classic microseepage theory. In this article, we introduce a novel collection of alteration products induced by a microseepage system using detailed examination of 360 hand samples collected 'on' and 'off' the Alborz oil field in Qom area, Iran. Our Lab spectroscopy and follow-up analysis using an in-house spectral processing package named AMISA demonstrated that smectites (montmorillonite, nontronite, and likely palygorskite), chlorite, carbonates (calcite, and probably ankerite), iron oxides/oxyhydroxides (goethite, ferrihydrite, hematite, and possibly maghemite), and sulphates (gypsum and in parts jarosite) are present as diagenetic alteration products over the HC affected zones. The introduced mineralogic assemblage can provide a new insight into microseepage theory that in combination with classic model can set benchmarks for the characterization of microseepage-induced alterations using remote sensing technology.

Keywords: Remote sensing, microseepage model, alteration, hydrocarbon exploration, spectroscopy.

1. Introduction

Seals above hydrocarbon (HC) reservoirs are not perfectly efficient. Therefore, light gaseous HCs leak to the surface in a near-vertical fashion and trigger an array of diagenetic physio-chemical and mineralogical changes in the soils and sediments overlying a HC accumulations. Such changes, which are believed to be induced by microbial and bacterial activities feeding on leaking HCs, are collectively described by microseepage theory. According to this theory, a microseepage system can bear the following signatures: (i) anomalous gas concentration; (ii) abnormality in microbial and geobotanical communities; (iii) mineralogical changes and bleached facies; (iv) electrochemical changes; (v) micromagnetic anomalies; and (vi) U-K radiation anomalies (Holysh and Toth 1996; Price 1986; Saunders et al. 1999; Tedesco 1995).

The detection of microseepage phenomenon is significant for oil and gas exploration, because it provides a conclusive evidence for the formation of petroleum system in a given sedimentary basin and, more importantly, because it supplies a powerful targeting tool for HC prospecting (Schumacher 2010, 2012). Owing to this significance, a diverse range of unconventional exploration methodologies has emerged to detect microseepage effects in direct or indirect manner.

One of the appealing technologies to track the footprints of microseepage systems is spectral remote sensing. This technique attempt to map the diagenetic minerals delineated by microseepage model using their diagnostic spectral features within the visible-near infrared (VNIR) and the shortwave infrared (SWIR) wavelengths (Lammoglia and Souza Filho 2013; Petrovic et al. 2012; Segal and Merin 1989; Shi et al. 2012). In particular, remote sensing data have been used to map an increase in the quantity of clays (kaolinite) and carbonates (calcite,

dolomite, and ankerite), and pervasive loss of ferric iron minerals (hematite) depicted as bedrock bleaching.

Whereas this suite of alteration mineralogy has been successfully mapped and delineated using multi-, and hyperspectral remote sensing, there has been certain cases of ambiguity in interpreting the resultant maps in the context of microseepage-induced changes. Several reasons such as improper sensing system or inappropriate processing approach can be attributed to this ambiguity; however, the authors believe that such issues can in part arise from inaccurate mineralogic targets as recommended by the classic model. In this article, we introduce a new suite of alteration products induced by microseepage systems through detailed examination of hand samples collected over Alborz oil field in the Qom area, Iran.

The Qom study area is located near the city of Qom, some 100 km to the south of Tehran, Iran. The test site encompasses an area of about 1450 km^2 within a back-arc sedimentary basin and includes the Alborz oil field in the form of a structural reservoir effectively sealed by very thick evaporitic sequence of late Miocene and covered by Oligocene sediments of the Upper Red Formation (Fig. 1) (Aghanabati 2004; Berberian and King 1981). The climate of this region is arid to semi-arid with less than 150 mm of average annual precipitation and thus embodies well exposed bedrocks (Fig. 2). The sandstone, siltstone, and claystone (collectively called sandstone henceforth) units of the URF vary in thickness from millimetric laminated strata to beds of several meters. On the petroliferous zones, this formation is commonly friable and porous with many cavities, hence very prone to mechanical weathering and erosion.

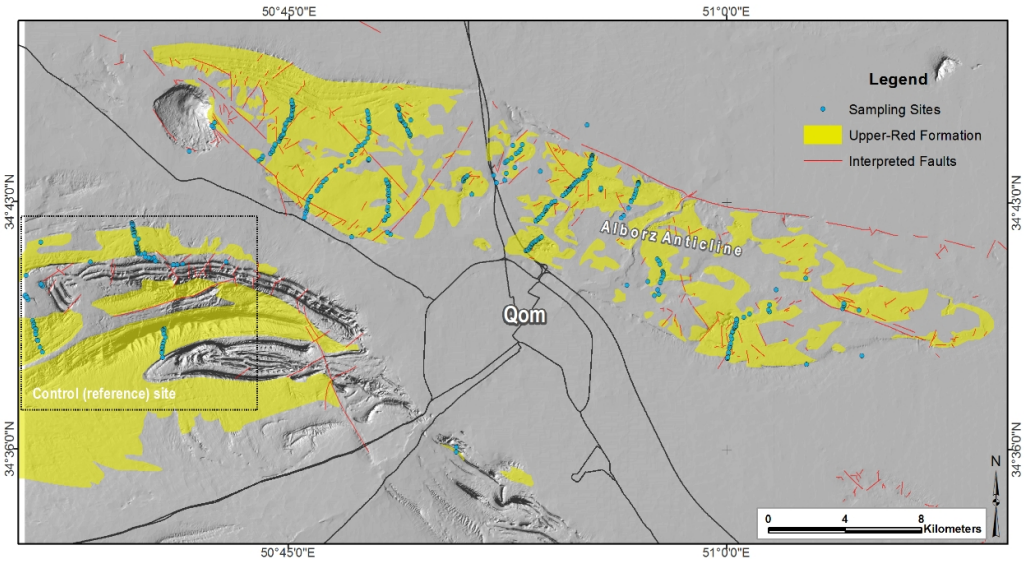

Figure 1. Simplified geologic map of the study area and the sampling sites superimposed on shaded relief topography.

2. Methodology

Field works was conducted during February 2011 to December 2012 along previously devised profiles perpendicular to stratigraphic variations. To draw a fair comparison, we covered areas ‘off’ the petroliferous terrain along with the main area ‘on’ the Alborz field respectively composed of altered and unaltered URF units. The former was used as reference site (Fig. 1) for evaluation of the results and diagenetic changes.

Overall, we collected some 360 samples in the area along 18 profiles, with an average of one sample per 120 m (Fig. 1). The samples cover a variety of targets including weathered and fresh lithologies (including sandstone, shale, marl, and gypsum) and associated soil

covers. The majority of the samples were collected from areas exposed to orbital sensors, but vertical faces hidden to sensors were also sampled. The sample suites were delivered to the Reflectance spectroscopy Lab of the University of Campinas (UNICAMP) for follow up spectral measurements.

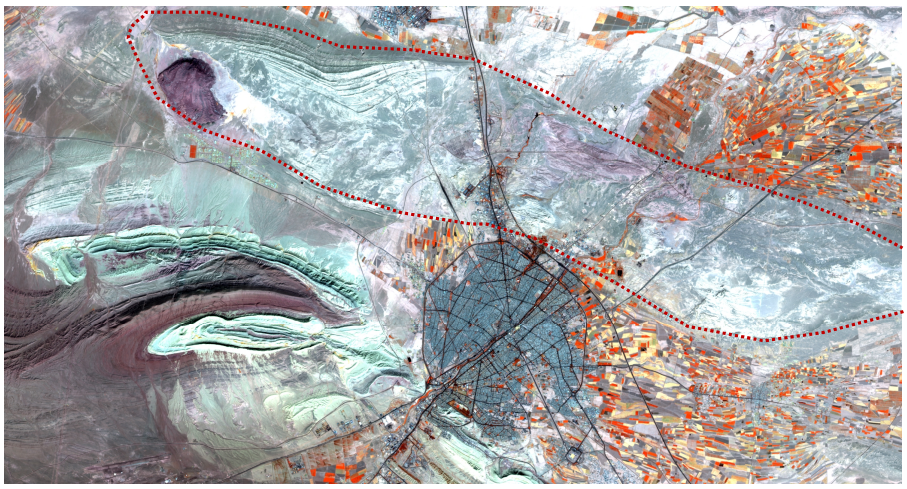

Figure 2. The outline of Alborz oil field (dashed red line) overlaid on Sentinel-2 color composite (RGB= b8, b11, b12) imagery.

In the Lab, we firstly recorded the color variations of selected samples using a Munsell color chart. Then, the entire sample suite was spectrally measured using a FieldSpec-4 spectrometer under artificial illumination from a contact probe and 1 nm sampling intervals between 350–2500 nm spectral range. For each measurement, we averaged 50 individual scans to minimize the contribution of instrumental noise. Subsequently, more than 2500 representative spectra were collected and corrected for splice drift. To analyze the dataset, we developed a series of routines in the Interactive Data language (IDL) program and named the collection 'Automated Absorption-based Mineral Spectral Analyzer' (AMISA). The package enables the calculation of wavelength of minimum, depth, width, area, and asymmetry of a given absorption feature in a fully automated fashion (Asadzadeh and Souza Filho 2016). All the diagnostic absorption features occurring in the VNIR–SWIR ranges were carefully defined and analyzed by the means of this in-house routine (Fig. 3).

3. Results and Discussion

It was observed that the originally dark reddish gray (10R, 4/1) sandstones were bleached to light gray (5Y, 7/1) beds due to the dissolution of iron oxide (hematite) coatings. The most common color degradation, however, was the transformation of red-beds into pale yellow (5Y, 8/2), due to neomineralization of iron oxyhydroxides species or changes in the abundance of ferric minerals.

The spectral analysis carried out by the AMISA package demonstrated that smectites (montmorillonite, nontronite, and likely palygorskite), chlorite, carbonates (calcite, and probably ankerite), iron oxides/oxyhydroxides (goethite, ferrihydrite, hematite, and possibly maghemite), and sulphates (gypsum and in parts jarosite) are present as diagenetic alteration products over the Alborz microseepage system. The original red-beds were characterized by an absorption feature centered at ~880 nm relevant to hematite, whereas samples collected

from petroliferous zones were mainly associated with a shift in this feature towards longer wavelengths (between ~890–930 nm) (Fig. 4a).

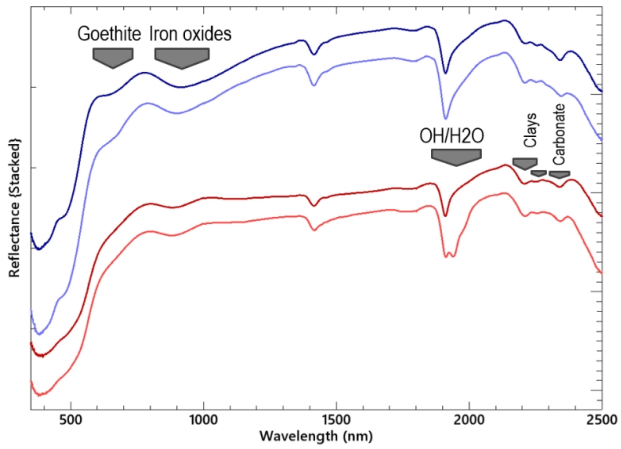

Figure 3. Examples of the collected spectra in the lab and the analyzed absorption features via AMISA routine.

Some altered samples were also showing a feature centered at ~650 nm, which is characteristic of goethite (Fig. 3). This change is presumably linked to the transformation of hematite into goethite and other metastable oxyhydroxides. This secondary ferric irons represent diffuse, banded, spotty, and irregular concretionary patterns visually. Remarkably, the noted transformation is associated with an increase in the depth of the absorption feature (Fig. 4b), along with a decrease in the feature asymmetry (Fig. 4c). The decrease in the asymmetry (equivalent to an increase in the area of the right wing of the feature) could be linked to overlapping ferrous features embedded in ankerite and/or chlorite, whereas, the increase in the deepened absorption is directly related to an increase in the amount of ferric iron in the environment. We postulate that this phenomenon is due to the accumulation of initially reduced ferrous iron into the lower sedimentary horizons and subsequent oxidation by meteoric water, which is not unlikely in an arid climate with low water table and pervasive vadose (oxidizing) zone. Such situation can be a reason behind the absence of pyrite deposits over petroliferous terrains.

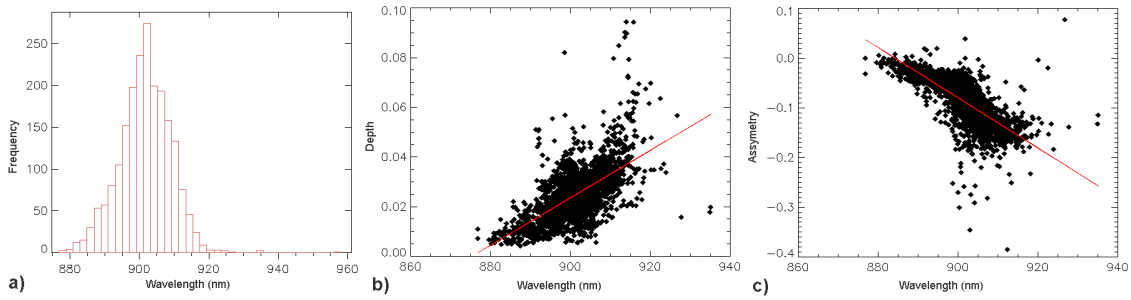

Figure 4. Characteristics of the ferric absorption feature at ~900 nm in the samples collected from Qom area. a) histogram of the wavelength minimum of the feature. b) variation of wavelength of minimum against depth calculated relative to fitted continuum. c) variation of wavelength of minimum against asymmetry calculated using the area of the absorption to the left and right of the minimum wavelength.

Thus far, kaolinite has not been observed in the sample suite; instead, we have detected a rich variety of clays in the microseepage-affected zones consisting of montmorillonite (with diagnostic absorption feature at ~2205 nm), nontronite (with distinctive feature at ~2290 nm), palygorskite (with a shift in OH absorption towards ~1415 nm), and intermediate Mg/Fe chlorite (with a feature centered at ~2250 nm).

Our analysis also revealed that calcite (feature centered at ~2340 nm) is the dominant carbonate mineral present in the samples, however, trace amounts of ankerite (with absorptions between 2332–2338 nm) has also been recorded. The former mineral is almost unique to the microseepage-affected zone and is absent in the control area. Over the Alborz area, carbonates seemingly have not contributed in re-cementation of the sandstones, because the carbonate-rich bleached facies are severely eroded. In contrast, where the gypsum (differentiated via its water absorption at ~1940 nm) is present, it substantially takes part in the cementation of the units and forms local highlands and cliffs. In such circumstances, gypsum shows a negative correlation with calcite abundance. This means that gypsum has been precipitated at the expense of calcite dissolution. Most likely, the oxidation of pyrite in high pH environment imposed by the occurrence of calcite can form gypsum and ferric hydroxides:

$$FeS_2 + 2\,CaCO_3 + 11/2\,H_2O + 15/4\,O_2 \;\text{à}\; Fe(OH)_3 + 2CaSO_4 \,.\, 2H_2O + 2CO_2$$

Pyrite Calcite Ferric hydroxide Gypsum

This finding can be consistent with the reasons provided for the excess of ferric irons. In the absence of carbonate buffering, the oxidation of pyrite was observed to form jarosite (with a distinctive feature at ~2270 nm) in some local veins.

4. Conclusion

A new series of mineralogic changes due to microseepage effects was described. In terms of clay alteration, alongside kaolinite, a microseepage system can generate different species of smectites and chlorites. The loss of ferric minerals delineated in classic model represent only one state of iron transformation. In arid to semi-arid climates where the water is scare and oxidation is pervasive, the ferric iron can go through different meta-stable phases without being transformed into permanent ferrous irons or flushed out of the system. Accordingly, aside the iron oxide abundance, the variation in its species (marked by a shift in absorption feature centered at ~900 nm) can be an exploration indicator for microseepage phenomenon. Despite some earlier studies that denoted the replacement of gypsum by calcite (Donovan 1974), we observed that pyrite in such systems can be weathered into gypsum at the expense of calcite dissolution. Indeed, the resulting sulphate minerals (e.g. gypsum and jarosite) can constitute new targeting signatures for remote sensing microseepage detection. Ultimately, the variation in carbonates species (from Ca to Fe, Mg, and Mn) can offer richer targets for microseepage delineation.

The next step in our study is to validate the spectroscopic results using a collection of analytical techniques such as X-ray diffraction (XRD), X-ray fluorescence (XRF), and optical microscopy and then map the noted alterations in local to regional scales using orbital remote sensing systems including Sentinel-2, WorldView-3, and ASTER instruments.

5. References

Aghanabati, A. (2004). **Geology of Iran** (in Persian). (First ed.). Tehran: Geological Survey of Iran.

Asadzadeh, S., & Souza Filho, C.R. (2016). Iterative Curve Fitting: A Robust Technique to Estimate the Wavelength Position and Depth of Absorption Features From Spectral Data. **IEEE Transactions on Geoscience and Remote Sensing**, 54, 5964-5974.

Berberian, M., & King, C.C.P. (1981). Toward a paleogeography and tectonic evolution of Iran. **Canadian Journal of Earth Sciences**, 18, 210-265.

Donovan, T.J. (1974). Petroleum Microseepage at Cement, Oklahoma; Evidence and Mechanism. **AAPG Bulletin**, 58, 429-446.

Holysh, S., & Toth, J. (1996). Flow of formation waters: Likely cause for poor definition of soil gas anomalies over oil fields in east-central Alberta. In D. Schumacher, & M.A. Abrams (Eds.), **Hydrocarbon migration and its near-surface expression** (pp. 255-277). Tulsa, OK, U.S.A.: AAPG Memoir 66.

Lammoglia, T., & Souza Filho, C.R. (2013). Unraveling Hydrocarbon Microseepages in Onshore Basins Using Spectral–Spatial Processing of Advanced Spaceborne Thermal Emission and Reflection Radiometer (ASTER) Data. **Surveys in Geophysics**, 34, 349-373.

Petrovic, A., Khan, S.D., & Thurmond, A.K. (2012). Integrated hyperspectral remote sensing, geochemical and isotopic studies for understanding hydrocarbon-induced rock alterations. **Marine and Petroleum Geology**, 35, 292-308.

Price, L.C. (1986). A critical review and proposed working model of surface geochemical exploration. In M.J. Davidson (Ed.), **Unconventional methods in exploration for petroleum and natural gas** (pp. 245–304). Dallas: Southern Methodist University Press.

Saunders, D.F., Burson, K.R., & Thompson, C.K. (1999). Model for hydrocarbon microseepage and related near-surface alterations. **AAPG Bulletin**, 83, 170-185.

Schumacher, D. (2010). Integrating hydrocarbon microseepage data with seismic data doubles exploration success. In, **34th annual conference and exhibition** (p. 11). Indonesia: Proceedings, Indonesian petroleum association.

Schumacher, D. (2012). Pre-drill prediction of hydrocarbon charge: Microseepage-based prediction of charge and post-survey drilling results. In, **CWLS GeoConvention 2012** (p. 9). Calgary, AB, Canada: AAPG.

Segal, D.B., & Merin, I.S. (1989). Successful use of Landsat Thematic Mapper data for mapping hydrocarbon microseepage-induced mineralogic alteration, Lisbon Valley, Utah. **Photogrammetric Engineering and Remote Sensing**, 55, 1137-1145.

Shi, P., Fu, B., Ninomiya, Y., Sun, J., & Li, Y. (2012). Multispectral remote sensing mapping for hydrocarbon seepage-induced lithologic anomalies in the Kuqa foreland basin, south Tian Shan. **Journal of Asian Earth Sciences**, 46, 70-77.

Tedesco, S.A. (1995). **Surface geochemistry in petroleum exploration**. New York: Chapman and Hall, Inc.